

Solution-Processable Ambipolar Diketopyrrolopyrrole–Selenophene Polymer with Unprecedentedly High Hole and Electron Mobilities

Junghoon Lee,^{†,§} A-Reum Han,^{‡,§} Jonggi Kim,[†] Yiho Kim,[†] Joon Hak Oh,^{*,‡} and Changduk Yang^{*,†}

[†]Interdisciplinary School of Green Energy and [‡]School of Nano-Bioscience and Chemical Engineering, KIER-UNIST Advanced Center for Energy, and Low Dimensional Carbon Materials Center, Ulsan National Institute of Science and Technology (UNIST), Ulsan 689-798, South Korea

Supporting Information

ABSTRACT: There is a fast-growing demand for polymer-based ambipolar thin-film transistors (TFTs), in which both *n*-type and *p*-type transistor operations are realized in a single layer, while maintaining simplicity in processing. Research progress toward this end is essentially fueled by molecular engineering of the conjugated backbones of the polymers and the development of process architectures for device fabrication, which has recently led to hole and electron mobilities of more than $1.0 \text{ cm}^2 \text{ V}^{-1} \text{ s}^{-1}$. However, ambipolar polymers with even higher performance are still required. By taking into account both the conjugated backbone and side chains of the polymer component, we have developed a dithienyl-diketopyrrolopyrrole (TDPP) and selenophene containing polymer with hybrid siloxane-solubilizing groups (PTDPPSe-Si). A synergistic combination of rational polymer backbone design, side-chain dynamics, and solution processing affords an enormous boost in ambipolar TFT performance, resulting in unprecedentedly high hole and electron mobilities of 3.97 and $2.20 \text{ cm}^2 \text{ V}^{-1} \text{ s}^{-1}$, respectively.



INTRODUCTION

Polymer semiconductors inherently facilitate solution processing and have the mechanical robustness necessary for flexible and ultralow-cost devices created by printing technologies.^{1–8} Polymer-based “electronic circuits” are expected to open up possibilities for ubiquitous electronics, including flexible displays,⁹ radio frequency identification (RFID) tags,¹⁰ and large-area sensors.¹¹ Through a combination of improved semiconducting polymer design^{1,2,12–14} and fabrication techniques,^{1,2,14–17} impressive progress has been made in enhancing the mobilities of organic thin-film transistors (OTFTs), reaching levels of $1–3.3 \text{ cm}^2 \text{ V}^{-1} \text{ s}^{-1}$,^{18–22} even exceeding $8 \text{ cm}^2 \text{ V}^{-1} \text{ s}^{-1}$ just recently²³ for unipolar *p*-channel operation and nearing $1.0 \text{ cm}^2 \text{ V}^{-1} \text{ s}^{-1}$ for unipolar *n*-channel operation.¹ Furthermore, advancements in complementary metal-oxide-semiconductor (CMOS)-like digital integrated circuits and organic light-emitting transistors (OLETs) have resulted in ambipolar TFTs capable of transporting both holes and electrons in one device.^{24–26} Owing to their simplicity of circuit design and fabrication processes, ambipolar TFTs with a dual-nature single semiconductor^{27–29} are superior to dual unipolar component systems, i.e., bilayers,²⁵ or bulk-heterojunction blends²⁶ for fulfilling the aforementioned requirements. Recently reported state-of-the-art ambipolar polymers have charge carrier mobilities for both holes and electrons ranging from 0.1 to $0.7 \text{ cm}^2 \text{ V}^{-1} \text{ s}^{-1}$.^{30,31} Mobilities exceeding $1.0 \text{ cm}^2 \text{ V}^{-1} \text{ s}^{-1}$ have even been observed with optimized annealing temperatures and contact electrode treatments.^{31,32} High-performance ambipolarity in ambient has also been observed from coronenediimide-based copolymers.³³

However, novel ambipolar polymers with better performance and further advances in fabrication processes are still required to truly realize practical organic integrated circuits based on single layers of ambipolar polymers.^{34,35}

In general, crystalline domains in the active layer are formed by the π -stacked conjugated backbone and macroscopic organization of the polymer and enhance charge carrier mobilities.^{2,4,20} A powerful strategy for achieving molecular packing with a large π -orbital overlap is the utilization of fused aromatic rings, in addition to donor–acceptor (D–A) diads,^{2,36–43} as the building blocks within the polymer backbone. This approach enhances effective π -conjugation, prevents chain folding, and narrows the bandgap, which facilitates the intermolecular charge transport.⁴⁴ However, such rigid and planar π -conjugated polymer frameworks tend to be insoluble. To maintain solution processability, long-branched alkyl solubilizing groups are introduced, which results in transient disruptions of molecular packing in the condensed phase and a reduction in the density of chromophores in the polymer.

Despite extensive research on conjugated polymer backbones,^{18,45–53} very little work has been done toward a coherent molecular design that can substantially govern intermolecular self-assembly by manipulating structural features such as the length, bulkiness, rigidity, and chirality of the solubilizing groups on the backbone. Recently, Bao et al. demonstrated the effectiveness of siloxane-terminated solubilizing groups as side chains in

Received: September 8, 2012

Published: November 23, 2012

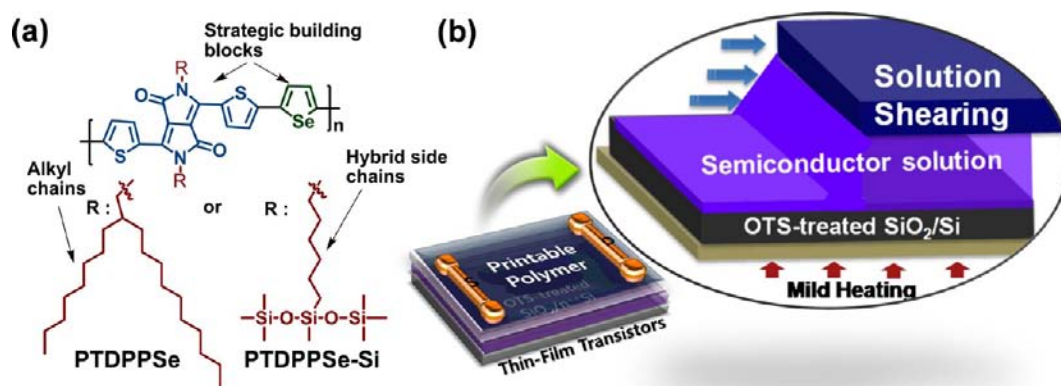


Figure 1. Design motif and solution-shearing schematic. (a) Molecular structures of PTDPPSe and PTDPPSe-Si and (b) schematic illustration of TFT structure and solution-shearing technique, in which a small volume of organic or polymer semiconductor solution is sandwiched between two preheated silicon wafers that move relative to each other at a controlled speed. This method yields crystalline and aligned thin films from various soluble organic or polymer semiconductors.

an isoindigo-containing polymer such as PII2T-Si for enhancing charge transport by inducing a denser π - π spacing and a larger crystalline coherence length.⁵⁴

Inspired by this initial discovery, we report a solution-processable D-A copolymer based on fused ring diketopyrrolopyrrole (DPP) consisting exclusively of the hybrid siloxane substituents at nitrogen atoms of the DPP motif, in which selenophene rings flank the DPP unit, abbreviated PTDPPSe-Si (Figure 1), and thoroughly describe its thin-film properties and transistor characteristics. The resulting polymer exhibited unprecedentedly high hole and electron mobilities of 3.97 and 2.20 $\text{cm}^2 \text{V}^{-1} \text{s}^{-1}$ in solution-sheared polymer films, illustrated schematically in Figure 1. To the best of our knowledge, these are the highest recorded hole and electron mobilities for organic- or polymer-based ambipolar TFTs reported to date.

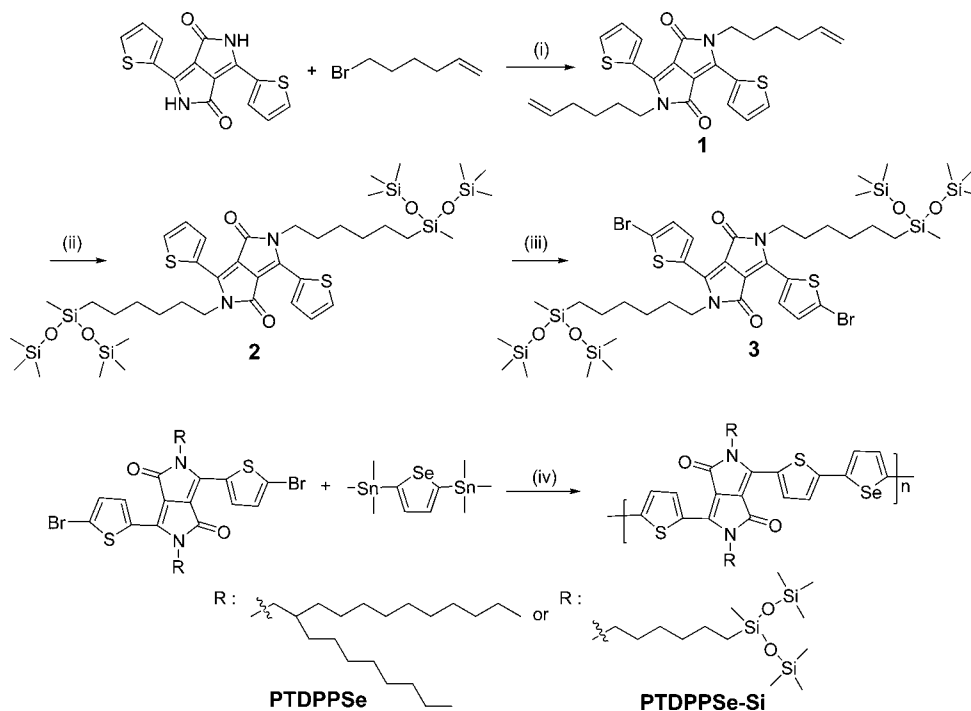
RESULTS AND DISCUSSION

Synthetic Strategies, Synthesis, and Characterization.

The strategy for further improvement in charge carrier mobility in comparison to the above-named PII2T-Si copolymer is to replace electron-deficient isoindigo building blocks with fused ring DPPs in which not only the carbonyl groups act to assist coplanarizing the appended neighboring thiophene units via short-contact oxygen-sulfur interactions but also the intermolecular interactions are promoted by the cross-axis dipoles.³¹ Furthermore, we decided to couple the thiophene-flanked DPP monomer (dithienyl-diketopyrrolopyrrole, TDPP) with an electron-rich selenophene unit into a D-A system since the selenophene-implanted polymers are anticipated to hold diverse advantages from the unique properties of the Se atom and selenophene:⁵⁵ (i) interchain-charge transfer should be facilitated by intermolecular Se...Se contacts;⁵⁶ (ii) oligo- and polyselenophenes should resist twisting along the main backbone due to a more quinoidal character;⁵⁷ (iii) the lower-energy LUMO of the selenophene motif should enhance electron transport by facilitating electron injection from metal electrodes. The lower LUMO should also lower the susceptibility of electron trapping and reaction with environmental oxidants.^{27,55,58,59} Therefore, a synergistic combination of effects produced through the incorporation of oligoselenophene and TDPP moieties in the solid state should contribute to the realization of high-mobility TFTs. Although a TDPP-thiophene copolymer with siloxane groups was reported very recently, the polymer thin films prepared with a droplet

pinning method exhibited conspicuously hole-dominant charge transport ($\mu_{\text{hole}} = 0.63 \text{ cm}^2 \text{V}^{-1} \text{s}^{-1}$ and $\mu_{\text{electron}} = 0.024 \text{ cm}^2 \text{V}^{-1} \text{s}^{-1}$) because of the electron-rich nature of the thiophene rings.²⁹ In addition to this D-A diad design (vide supra), special attention was paid to the influence of the hybrid siloxane side chains in the polymer. Such substituents enforce long-range molecular arrangements through the minimization of steric repulsion between side chains. This promotes smaller π - π stacking distances.

Synthesis of the intermediates and the target polymer (PTDPPSe-Si) was carried out, depicted in Scheme 1 (see full synthetic details and characterization in the Experimental Section and Supporting Information). For the sake of comparison, a TDPP-selenophene copolymer (PTDPPSe) with long branched alkyl side chains (2-octyldodecyl) as the reference polymer was also prepared according to established literature procedures.⁶⁰ The synthesis began with a standard N-alkylation of TDPP with 6-bromo-1-hexene under basic conditions, and subsequent hydrosilylation reaction of the olefinic compound **1** using 1,1,1,3,5,5,5-heptamethyltrisiloxane gave the siloxane-substituted precursor **2** in the presence of Karstedt catalyst,⁶¹ which was then converted to the dibrominated TDPP **3** as a monomer for metal (Ni or Pd)-catalyzed cross-coupling polymerizations. A Stille copolymerization of the dibrominated TDPP **3** and distannylated selenophene⁶² generated the target D-A polymer PTDPPSe-Si. The resulting polymers were purified by precipitation into methanol followed by Soxhlet extraction using methanol, acetone, hexane, and finally chloroform. Satisfactory molecular weights were obtained in both cases (M_n of 122.3 and 269.4 kg/mol with polydispersity indices (PDI) of 3.58 and 4.38 for PTDPPSe and PTDPPSe-Si, respectively, as determined by gel-permeation chromatography vs PS standard, THF eluent). Both polymers were readily soluble in conventional organic solvents (THF, chloroform, toluene, etc.) at room temperature. To rule out a misleading molecular weight value causable by polymer aggregates, molecular weights were redetermined using a high-temperature gel-permeation chromatography (GPC) at 150 °C with 1,2,4-trichlorobenzene as eluent. This experiment revealed a M_n of 18.0 and 20.3 kg/mol for PTDPPSe and PTDPPSe-Si, respectively, with a PDI of 3.85 and 4.93. This implies only a small difference between the molecular weights of PTDPPSe and PTDPPSe-Si under normal conditions without forming aggregates.

Scheme 1. Synthetic Route to PTDPPSe and PTDPPSe-Si^a

^aReagents and conditions: (i) K_2CO_3 , DMF, 100 °C, 82%; (ii) Karstedt catalyst, 1,1,1,3,5,5,5-heptamethyltrisiloxane, toluene, 50 °C, 79%; (iii) NBS, $CHCl_3$, dark, rt, 21%; (iv) $Pd_2(dba)_3$, $P(o-tol)_3$, toluene, 95 °C, 75%.

The absorption spectra of PTDPPSe dissolved in chlorobenzene and cast in a thin film were similar in shape to a broad absorption maximum (λ_{max}) centered at 805 nm. However, a pronounced red-shift of the absorption onset (~ 30 nm) was observed when going from solution to the solid state, indicating greater intermolecular interactions in the solid state (Figure 2a). A solution of PTDPPSe-Si yielded an absorption maximum at 845 nm and exhibited a 45 nm red-shift of the adsorption onset with respect to the reference polymer solution (Figure 2a and b). This indicates a preorganization of the polymer chains via strong π - π stacking of the D-A diads and can be attributed to the minimization of steric effects between side chains because the branching point of the heptamethyltrisiloxyl groups is sufficiently far away from the conjugated backbone. Note that the corresponding thin-film absorption showed a slight blue-shift relative to the solution spectrum (Figure 2b). This effect has been observed with other indigo- and TDPP-based polymers.^{6,54,63} This unexpected formation of H-type aggregate currently lacks a logical explanation but might be attributed, in part, to the interaction between the polar siloxane chains and the TDPP-selenophene main backbone in the solid state. It has been reported that strong polar interactions between TDPP-based polymers that can consist of H-bonding induce a blue-shift.⁶⁴ We are currently studying the different optical features of TDPP-based polymers as a function of various side-chain dynamics. Both polymers exhibited nearly identical optical band gaps of approximately 1.2 eV, as determined from the absorption edges in their thin film spectra (Figure 2).

The HOMO levels of thin films of both polymers were measured by ultraviolet photoelectron spectroscopy (UPS) (Figure 3a and b). The ionization potential (IP, |HOMO|) is determined by using the incident photon energy ($h\nu = 21.2$ eV) for He I, E_{cutoff} and E_{HOMO} according to the equation, $IP = h\nu - (E_{cutoff} - E_{HOMO})$.⁶⁵ The electron affinity (EA, |LUMO|) is

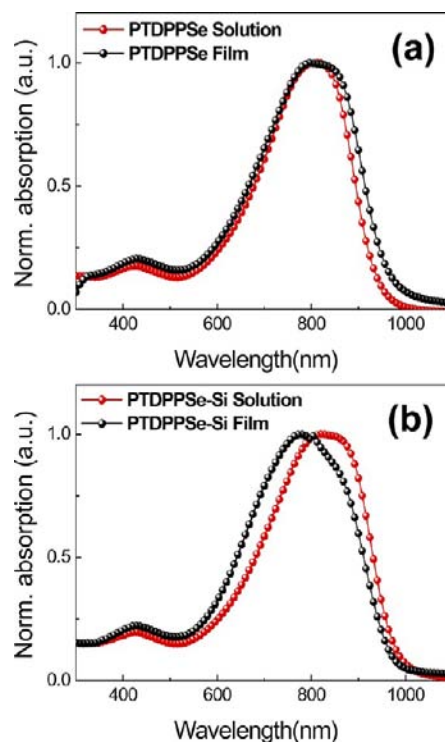


Figure 2. UV-vis-NIR absorption spectra of (a) PTDPPSe and (b) PTDPPSe-Si in dilute chlorobenzene solution and thin films on a quartz plate.

estimated by using the HOMO and the optical gap from the UV-vis-NIR absorption from Figure 2. The replacement of aliphatic side chains with hybrid siloxane chains in the polymer backbone increased both the HOMO and LUMO energy levels

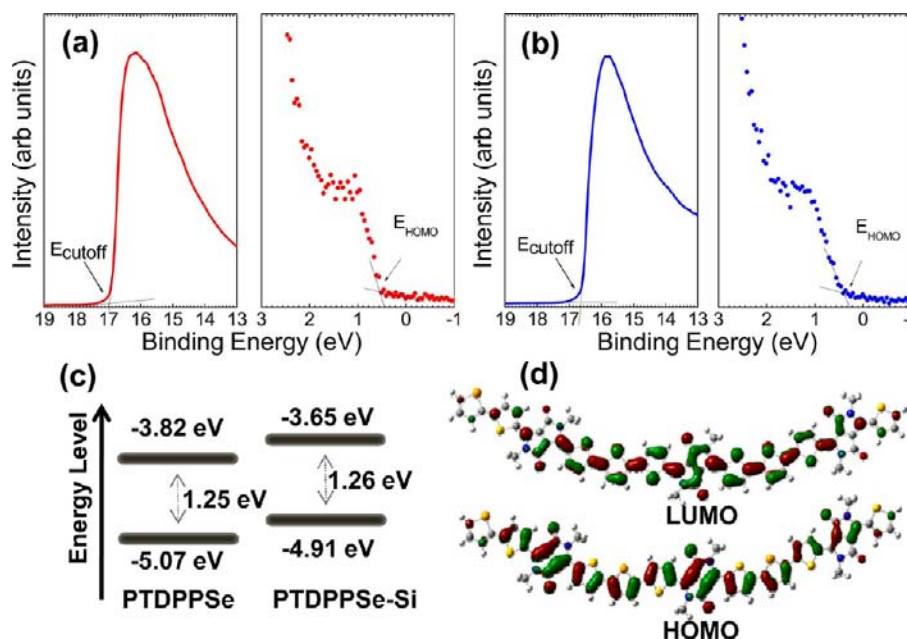


Figure 3. Ultraviolet photoelectron spectroscopy (UPS) spectra of (a) PTDPPSe and (b) PTDPPSe-Si. A gold film 75 nm thick was deposited on a precleaned Si substrate with a thin native oxide. (c) Energy level diagrams for TDPPSe-based copolymers. (d) DFT-optimized geometries and charge-density isosurfaces for the LUMO and HOMO levels of the methyl-substituted TDPPSe trimer containing methyl side chains.

(−5.07 and −3.82 eV for PTDPPSe and −4.91 and −3.65 eV for PTDPPSe-Si, respectively, see Figure 3c). The observed energy level differences are indicative of packing effects in the solid state. Note that deviations from coplanarity result in shorter effective π -conjugation lengths and lower HOMO levels.⁶⁶ Therefore, the tethered siloxane substituents in PTDPPSe-Si promote organization of the polymer backbone, which is in good agreement with the absorption features described above. The HOMO levels estimated by cyclic voltammetry show a similar trend for PTDPPSe-Si over PTDPPSe (see Supporting Information).⁵⁴ In the present or expanded cases associated with the D–A based molecular design, one can conclude that the nature of D–A chromophores within the polymers is not an entirely definitive answer to the energy levels.

To elucidate the electron state density distributions of the HOMO and LUMO levels of geometry-optimized structures based on a TDPP and selenophene repeating unit, computational studies using density-functional theory (DFT, B3LYP/6-31G) were performed on a model trimeric system with alkyl chains replaced by methyl groups for simplicity. As shown in Figure 3d, both the HOMO and LUMO isosurfaces are spread over the whole conjugated backbone. Note that this contrasts with most other D–A polymers, in which the LUMOs are localized upon the electron-deficient core of the polymer backbone. Therefore, TDPP-selenophene polymer-based TFTs are expected to exhibit excellent ambipolar behaviors (vide infra).

Thin-Film Microstructure Analyses. Out-of-plane X-ray diffraction (XRD) analyses were performed to investigate the crystallinity and molecular organization in thin films of PTDPPSe and PTDPPSe-Si. Figure 4 shows diffractograms as a function of annealing temperature, and the XRD data of the thin films are summarized in Table 1. The as-cast PTDPPSe thin film exhibited a relatively broad primary diffraction peak at $2\theta = 4.17^\circ$, corresponding to a $d(001)$ -spacing of 21.16 Å. The PTDPPSe film annealed at 220 °C showed an intense and sharp primary diffraction peak at $2\theta = 4.21^\circ$, corresponding to a smaller $d(001)$ -spacing value of 20.95 Å. This indicates the formation of a highly

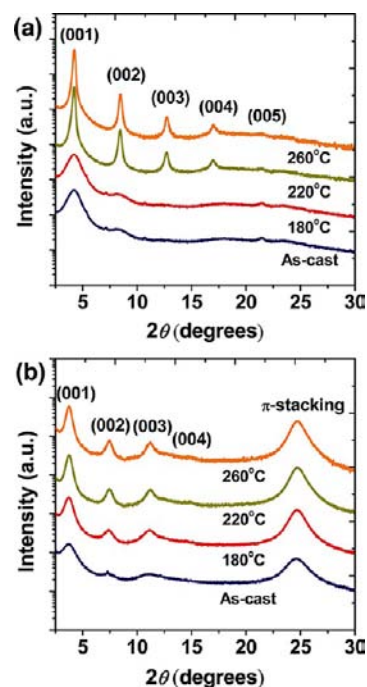


Figure 4. Out-of-plane X-ray diffraction (XRD) patterns of (a) PTDPPSe and (b) PTDPPSe-Si thin films, depending on annealing temperature.

ordered and denser molecular packing in the annealed film. Higher-order diffraction peaks were observed at $2\theta = 8.47^\circ$, 12.72° , 17.01° , and 21.43° , corresponding to (002), (003), (004), and (005) peaks, respectively. This implies that the annealed PTDPPSe film had long-range order across its thickness. The PTDPPSe-Si thin film also formed a denser molecular packing at higher annealing temperatures (see Table 1). The $d(001)$ -spacing value of the PTDPPSe-Si thin film annealed at 220 °C was reduced from 23.93 Å ($2\theta = 3.69^\circ$) to

Table 1. Peak Assignments for the Out-of-Plane XRD Patterns Obtained from PTDPPSe and PTDPPSe-Si Thin Films Depending on the Annealing Temperature

$T_{\text{annealing}}$	(00 <i>n</i>)	PTDPPSe		PTDPPSe-Si	
		2θ (°)	$d(001)$ -spacing (Å)	2θ (°)	$d(001)$ -spacing (Å)
as-cast	(001)	4.17	21.16	3.69	23.93
	(002)	8.06	-	7.30	-
	(003)	-	-	11.09	-
	(005)	21.35	-	-	-
	π -stacking ^a	23.52	3.78	24.67	3.61
180 °C	(001)	4.17	21.16	3.71	23.80
	(002)	8.29	-	7.38	-
	(003)	12.52	-	11.15	-
	(004)	16.77	-	14.43	-
	π -stacking	23.54	3.78	24.67	3.61
220 °C	(001)	4.21	20.95	3.75	23.54
	(002)	8.47	-	7.48	-
	(003)	12.72	-	11.21	-
	(004)	17.01	-	14.88	-
	(005)	21.43	-	-	-
260 °C	π -stacking	23.52	3.78	24.73	3.60
	(001)	4.23	20.85	3.75	23.54
	(002)	8.49	-	7.46	-
	(003)	12.74	-	11.23	-
	(004)	17.01	-	14.88	-
	(005)	21.37	-	-	-
	π -stacking	23.77	3.74	24.77	3.59

^aThe intensity of π -stacking for the PTDPPSe thin film was relatively weak, which exhibited a longer π -stacking distance of 3.7 Å compared to the PTDPPSe-Si thin film (3.6 Å).

23.54 Å ($2\theta = 3.75^\circ$), which is relatively larger than that (20.95 Å) of the PTDPPSe thin film. Well-defined, higher-order peaks were also observed at $2\theta = 7.48^\circ$, 11.21° , and 14.88° , corresponding to (002), (003), and (004) peaks, respectively. This is likely due to the longer bond length of Si–O (1.64 Å) relative to C–C (1.53 Å), despite the minimization of steric repulsions by the hybrid siloxane side chains. Interestingly, an additional and remarkably strong peak was observed at $2\theta = \sim 25^\circ$ in diffractograms of the PTDPPSe-Si thin films, regardless of annealing temperature. This can be attributed to the formation of efficient π - π stacking (π -stack distance ~ 3.6 Å) with face-on orientations. It is therefore expected that PTDPPSe-Si films would be able to adopt 3-D conduction channels that would enhance charge transport over that of polymer films with only perpendicular π - π planes.⁶⁷

To further shed light on the difference in the crystallinity and microstructure of the annealed films of PTDPPSe and PTDPPSe-Si, the morphologies of the polymer thin films were investigated using tapping-mode atomic force microscopy (AFM) and transmission electron microscopy (TEM). The AFM images of these drop-cast polymer thin films annealed at 220 °C revealed that the PTDPPSe thin film formed fine, isotropic “granular” (~ 40 nm in diameter) domains with a root-mean-square (rms) roughness value of 0.88 nm (obtained from the corresponding height image), whereas the PTDPPSe-Si thin film formed rugged granular structures with larger sizes (~ 100 nm in the long axis), implying the formation of more efficient pathways for charge carrier transport in the polymer film (Figure 5a and b). On the other hand, the solution-sheared PTDPPSe film exhibited the formation of similarly fine, but denser, grains, whereas the solution-sheared PTDPPSe-Si film

showed slightly larger granular domains (~ 120 nm in the long axis) (Figure 5c and d). In addition, the large-area AFM scans showed that the solution-sheared PTDPPSe-Si film formed directional valleys and large interconnected fibrillar domains (Figure 5e and f). AFM phase images and TEM images of the solution-sheared films of both polymers revealed that the PTDPPSe-Si thin film exhibits interconnected nanofibrillar structures when compared with the PTDPPSe thin film (see Figure S2 in Supporting Information). Therefore, one can conclude that the replacement of aliphatic side chains with hybrid siloxane chains in the polymer backbone results in different molecular packing behaviors in TDPP-selenophene copolymer films upon utilizing the solution-shearing process. It is expected from these morphological studies that the dense fibrillar domains composed of fused granules in the solution-sheared PTDPPSe-Si construct the interconnected networks of the polymer chains, leading to the formation of more efficient pathways for charge carrier transport in the polymer film.

Fabrication of Solution-Processed TFTs and I - V Characterizations. To demonstrate the effects of hybrid siloxane side chains on charge transport, we fabricated bottom-gate, top-contact TFTs based on PTDPPSe and PTDPPSe-Si. The polymer thin films (~ 35 nm thickness) were prepared on OTS-modified SiO₂/Si substrates from a TDPP-selenophene copolymer solution in chlorobenzene (5 mg mL⁻¹) using various solution-processing methods: spin-coating, drop-casting, and solution-shearing. The devices consisted of the insulator capacitance (10 nF cm⁻²), channel length (typically ~ 50 μm with the W/L ratio of 20), and Au source/drain electrodes (~ 40 nm) (see SI for the detailed information). The transport characteristics were measured in a nitrogen-filled glovebox. In the solution-shearing method (see Figure 1b), a small volume of polymer semiconductor solution is sandwiched between two silicon wafers preheated at a mild temperature (less than the boiling point of solvent).^{68–70} Then, a shearing plate drags the solution at a controlled speed while keeping the bulk of the solution between the plate and the substrate. The experimental details regarding surface modification and TFT fabrication are included in the Supporting Information. The TFT performances of PTDPPSe and PTDPPSe-Si are listed in Table 2, and the mobility variations as a function of the annealing temperature are shown in Figure S3 (Supporting Information). Both PTDPPSe and PTDPPSe-Si exhibited ambipolar characteristics, as expected from DFT calculations of TDPP-selenophene copolymers. The solution-sheared polymer thin films exhibited the best electrical performance among the solution-processed films, most likely due to the highly crystalline and aligned nature of solution-sheared films.^{68–70} The optimal annealing temperature was ~ 220 °C.

Figure 6 shows typical transfer and output characteristics of TFTs based on PTDPPSe and PTDPPSe-Si thin films annealed at 220 °C for 30 min in a nitrogen atmosphere. These TFT devices exhibited a small degree of hysteresis in both transfer and output curves. Both polymers exhibited the typical V-shape ambipolar transfer curves. The as-cast, solution-sheared PTDPPSe films showed the highest hole and electron mobilities of 0.14 and 0.05 cm² V⁻¹ s⁻¹, respectively. The hole mobility in PTDPPSe was approximately an order of magnitude higher than the electron mobility, which may be the result of a smaller injection barrier for holes with respect to the gold contacts. After annealing at 220 °C, the hole and electron mobilities increased to 2.53 and 0.43 cm² V⁻¹ s⁻¹, respectively, due to the formation of a denser molecular packing, as observed by XRD and AFM analyses.

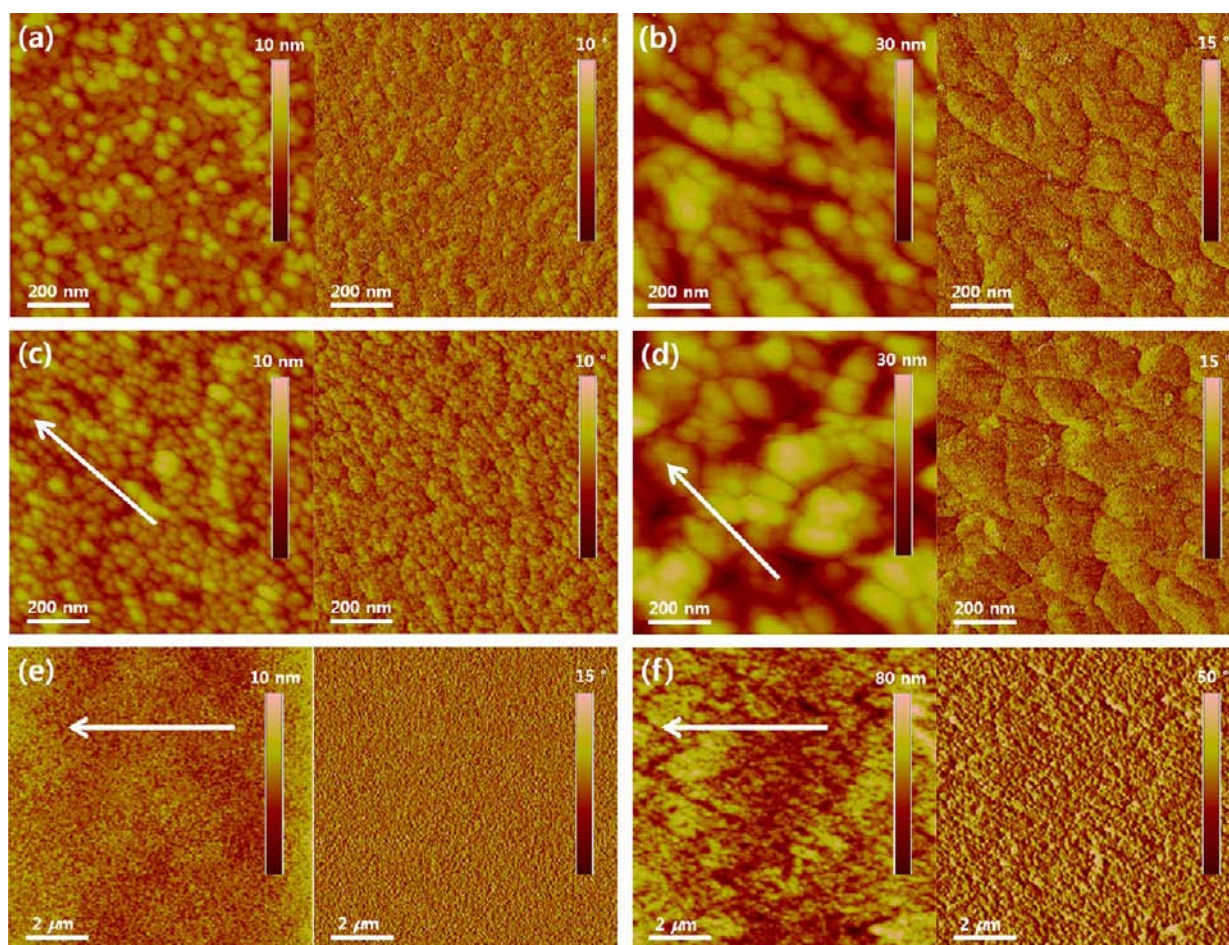


Figure 5. AFM height (left) and phase (right) images of {(a),(c),(e)} PTDPPSe and {(b),(d),(f)} PTDPPSe-Si films by {(a),(b)} drop-casting and {(c)-(f)} solution-shearing methods after annealing at 220 °C. The arrow indicates the direction of shearing.

Surprisingly, the as-cast, solution-sheared PTDPPSe-Si films showed very high hole and electron mobilities of 3.16 and 0.37 $\text{cm}^2 \text{V}^{-1} \text{s}^{-1}$, respectively. Furthermore, extraordinarily high hole and electron mobilities of 3.97 and 2.20 $\text{cm}^2 \text{V}^{-1} \text{s}^{-1}$ were obtained from PTDPPSe-Si films annealed at 220 °C. To the best of our knowledge, these are among the highest ambipolar mobilities, obtained with relatively well-balanced polarities, reported to date. It is noteworthy that enhancements in molecular ordering by solution-shearing and postannealing yielded greater electron mobilities, closing the gap in mobility between holes and electrons. Note that the electron mobility of PTDPPSe-Si films increased as the solution deposition method was changed from spin-coating to drop-casting or to solution-shearing methods. This phenomenon is probably closely related to the lower LUMO energy levels enabled by the enhanced molecular packing, which results in the smaller injection barriers for electrons with regard to the gold contacts.^{70,71}

The effects of annealing temperature on the ambipolar charge transport behaviors of PTDPPSe and PTDPPSe-Si TFTs were also investigated (see Figure S4 in Supporting Information). The superior charge transport performance of the PTDPPSe-Si TFTs can be attributed to improved coplanarity and stronger intermolecular interactions in the polymer film through the incorporation of hybrid siloxane-solubilizing groups. This conclusion is consistent with the results of the XRD and morphological analyses. The electron mobility was more sensitive to the annealing temperature than the hole mobility. Among the many possible

factors, we cannot rule out the extrinsic effects such as the oxygen/water contamination acting as electron traps.^{15,71,72} After annealing the polymer thin films, the trap density in the polymer would be relatively reduced, and it can result in the enhanced electron transport compared to the as-prepared film.³¹ In addition, the observation of the balanced ambipolar OFETs by increasing annealing temperature has been reported,⁶³ where the hole mobility was independent of the annealing temperature, while the electron mobility increased steadily with increasing annealing temperature. The increase in electron mobility was attributed to the polymer reorganization after phase transition resulting in a microstructure more favorable for electron transport.⁶³ Therefore, in addition to the energetic considerations, morphological virtues proven by the formation of larger grains in PTDPPSe-Si than PTDPPSe might also be related to the enhanced electron transport.

CMOS-like inverters based on two identical ambipolar transistors of PTDPPSe and PTDPPSe-Si were constructed using a common gate electrode for applying the input voltage (V_{IN}). The output voltage (V_{OUT}) was monitored as a function of V_{IN} at a constant supply bias (V_{DD}). Figure 7 shows the voltage transfer characteristic (VTC) curves. PTDPPSe and PTDPPSe-Si ambipolar semiconductors yielded a high gain of 16.2 and 18.0, respectively. Although the asymmetry in mobility and threshold voltage in *p*- and *n*-channel modes resulted in a hysteresis between forward and reverse sweeps for both polymers, PTDPPSe-Si exhibited a relatively smaller hysteresis because of the better balance between hole and electron mobilities.⁷³

Table 2. TFT Performance of PTDPPSe and PTDPPSe-Si

condition ^a			<i>p</i> -channel			<i>n</i> -channel		
polymer	films	T_a [°C]	$\mu_{h,max}$ [cm ² V ⁻¹ s ⁻¹]	$\mu_{h,avg}$ ^b [cm ² V ⁻¹ s ⁻¹]	I_{on}/I_{off}	$\mu_{e,max}$ [cm ² V ⁻¹ s ⁻¹]	$\mu_{e,avg}$ ^b [cm ² V ⁻¹ s ⁻¹]	I_{on}/I_{off}
PTDPPSe	spin-coated	N/A ^c	4.70×10^{-2}	$4.23 \times 10^{-2} (\pm 0.003)^d$	$>10^6$	5.86×10^{-3}	$5.17 \times 10^{-3} (\pm 0.0005)$	$>10^4$
		180	0.66	0.17 (± 0.20)	$>10^6$	7.81×10^{-2}	$7.03 \times 10^{-2} (\pm 0.010)$	$>10^4$
		220	1.36	1.02 (± 0.14)	$>10^5$	0.13	0.10 (± 0.01)	$>10^3$
		260	0.67	0.54 (± 0.08)	$>10^4$	7.25×10^{-2}	$6.88 \times 10^{-2} (\pm 0.0004)$	$>10^3$
	drop-cast	N/A	0.11	0.07 (± 0.03)	$>10^5$	1.42×10^{-2}	$1.08 \times 10^{-2} (\pm 0.002)$	$>10^2$
		180	0.35	0.30 (± 0.02)	$>10^5$	0.10	0.07 (± 0.01)	$>10^3$
		220	1.98	1.50 (± 0.35)	$>10^5$	0.38	0.21 (± 0.11)	$>10^3$
		260	1.44	1.36 (± 0.10)	$>10^5$	0.23	0.14 (± 0.05)	$>10^3$
	solution-sheared	N/A	0.14	0.09 (± 0.03)	$>10^5$	5.00×10^{-2}	$4.20 \times 10^{-2} (\pm 0.007)$	$>10^3$
		180	0.58	0.42 (± 0.12)	$>10^6$	0.12	0.08 (± 0.03)	$>10^3$
		220	2.53	2.48 (± 0.08)	$>10^5$	0.43	0.35 (± 0.11)	$>10^3$
		260	1.61	1.55 (± 0.12)	$>10^6$	0.23	0.16 (± 0.03)	$>10^4$
PTDPPSe-Si	spin-coated	N/A	0.59	0.46 (± 0.15)	$>10^4$	4.58×10^{-2}	$4.19 \times 10^{-2} (\pm 0.003)$	>10
		180	0.95	0.81 (± 0.09)	$>10^6$	6.69×10^{-2}	$5.89 \times 10^{-2} (\pm 0.017)$	$>10^2$
		220	1.69	1.54 (± 0.10)	$>10^5$	0.20	0.14 (± 0.04)	$>10^2$
		260	1.38	1.30 (± 0.13)	$>10^5$	0.15	0.13 (± 0.02)	$>10^2$
	drop-cast	N/A	1.07	0.98 (± 0.11)	$>10^5$	9.49×10^{-2}	$9.17 \times 10^{-2} (\pm 0.009)$	$>10^3$
		180	1.14	1.08 (± 0.05)	$>10^4$	0.20	0.16 (± 0.03)	>10
		220	2.48	2.02 (± 0.38)	$>10^5$	0.78	0.26 (± 0.24)	$>10^2$
		260	0.98	0.87 (± 0.11)	$>10^5$	9.26×10^{-2}	$9.04 \times 10^{-2} (\pm 0.004)$	>10
	solution-sheared	N/A	3.16	2.87 (± 0.26)	$>10^5$	0.37	0.18 (± 0.10)	$>10^2$
		180	3.23	3.16 (± 0.17)	$>10^6$	0.79	0.65 (± 0.13)	$>10^4$
		220	3.97	3.48 (± 0.30)	$>10^4$	2.20	0.97 (± 0.50)	>10
		260	2.27	1.99 (± 0.25)	$>10^4$	1.21	0.93 (± 0.33)	$>10^2$

^aThe *p*-channel and *n*-channel characteristics of ambipolar TFTs were measured with $V_{DS} = -100$ and $+100$ V, respectively. ^bThe average mobility of the TFT devices ($L = 50 \mu\text{m}$ and $W = 1000 \mu\text{m}$). ^cThe thermal annealing was not applied (as-prepared thin films). ^dThe standard deviation.

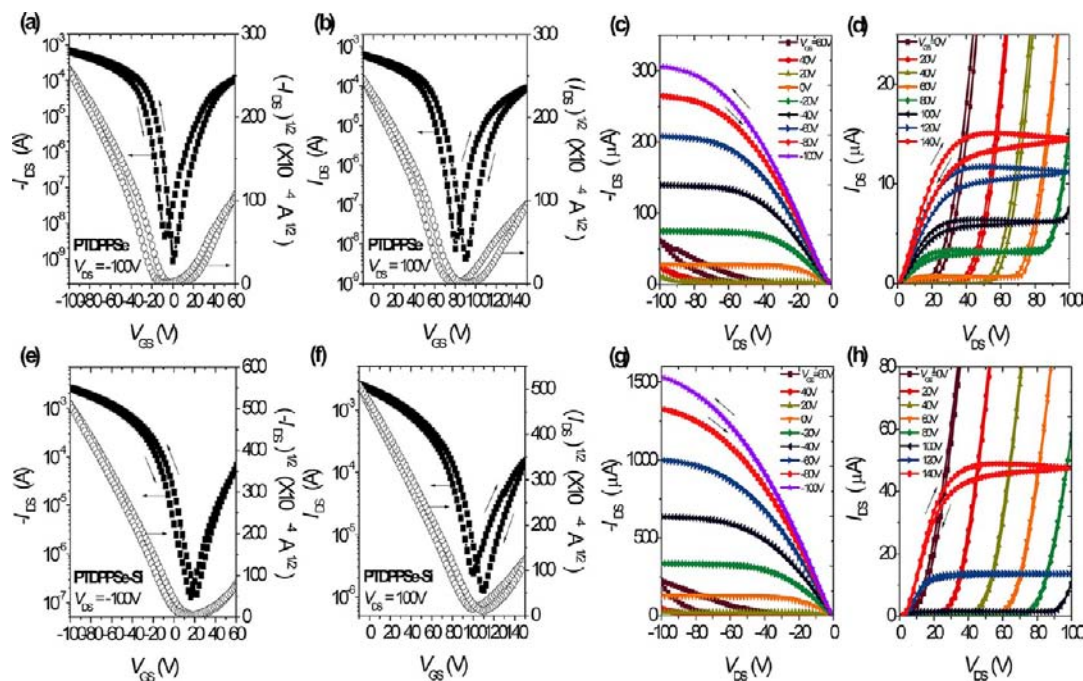


Figure 6. Current–voltage (I – V) characteristics of TFTs. {(a)–(d)} PTDPPSe and {(e)–(h)} PTDPPSe-Si solution-sheared thin films annealed at 220 °C. Transfer characteristics at {(a),(e)} hole-enhancement operation, $V_{DS} = -100$ V, and {(b),(f)} electron-enhancement operation, $V_{DS} = 100$ V. {(c),(d),(g), and (h)} Output characteristics of TDPP-selenophene copolymers ($L = 50 \mu\text{m}$ and $W = 1000 \mu\text{m}$).

CONCLUSION

Through rational molecular design of both the conjugated backbone and side chains, a D–A TDPP-selenophene copolymer (PTDPPSe-Si) bearing siloxane-terminated solubilizing groups

was synthesized. Unprecedentedly high hole ($3.97 \text{ cm}^2 \text{ V}^{-1} \text{ s}^{-1}$) and electron mobilities ($2.20 \text{ cm}^2 \text{ V}^{-1} \text{ s}^{-1}$) with relatively well-balanced polarities were observed in PTDPPSe-Si TFTs. These enhancements were due to a synergistic combination of the

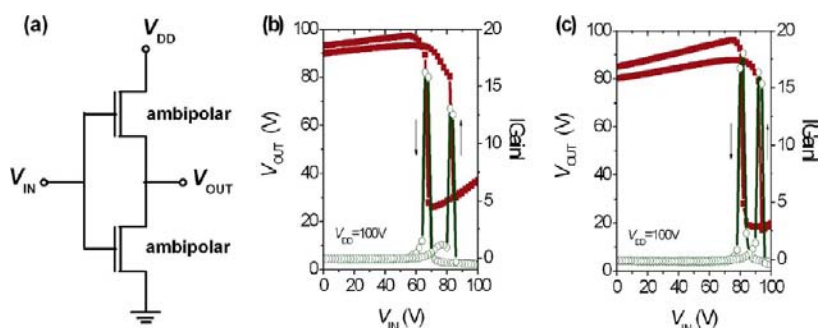


Figure 7. (a) Schematic of the complementary inverter structure. CMOS-like inverter characteristics of (b) PTDPPSe and (c) PTDPPSe-Si inverter ($V_{DD} = 100$ V).

rational molecular design of the polymer backbone, side-chain dynamics, and solution-processing techniques. Our results demonstrate that modifications to molecular packing through side-chain engineering, i.e., hybrid siloxane-side chains, can be used to effectively control the π - π stacking distance of conjugated polymers. This technique provides an alternative to manipulating the D-A backbones for tuning charge transport characteristics. The protocol developed herein can be extended to other state-of-the-art polymer backbones for the production of practical plastic electronics.

EXPERIMENTAL SECTION

Typical Procedure for Stille Polymerization and Polymer Purification. Dibrominated TDPP (0.20 mmol), distannyl selenophene comonomer (0.20 mmol), tris(dibenzylidenacetone)dipalladium (0) (1.7 mg, 2.0 μ mol), and anhydrous toluene (4 mL) were mixed in a Schlenk flask which was purged with argon for 30 min. To this solution, tri(*o*-tolyl)phosphine (1.2 mg, 4.0 μ mol) was added, and the reaction mixture was heated at 95 °C under vigorous stirring for 48 h. The crude product was poured into a mixture of methanol (300 mL). The resulting solid was filtered off and subjected to sequential Soxhlet extraction with methanol (1 day), acetone (1 day), and hexane (1 day) to remove the low molecular weight fraction of the materials. The residue was extracted with chloroform to produce a dark purple product after precipitating again from methanol and drying in vacuo.

Poly-3,6-dithien-2-yl-2,5-di(2-octyldecyl)-pyrrolo[3,4-c]pyrrole-1,4-dione-5',5''-diyl-alt-3-(5-(selenophene-2-yl)) (PTDPPSe). Isolated yield of polymer PTDPPSe = 150 mg (75%). GPC analysis $M_n = 122.3$ kg/mol, $M_w = 441.1$ kg/mol, and PDI = 3.58 (against PS standard) obtained by room-temperature GPC and $M_n = 18.0$ kg/mol, $M_w = 64.5$ kg/mol, and PDI = 3.58 (against PS standard) measured by high-temperature GPC at 150 °C with 1,2,4-trichlorobenzene as eluent. $^1\text{H NMR}$ ($\text{C}_2\text{D}_2\text{Cl}_4$, 600 MHz, 348 K): δ ppm 9.25–8.71 (br, 2H), 7.37–6.68 (br, 4H), 4.22–3.66 (br, 4H), 2.08–1.73 (br, 2H), 1.42–1.06 (br, 64H), 0.85–0.78 (br, 12H). Anal. Calcd for $\text{C}_{58}\text{H}_{90}\text{N}_2\text{O}_2\text{S}_2\text{Se}$: C, 70.33; H, 9.16; N, 2.83. Found: C, 70.61; H, 8.97; N, 2.63.

Poly-3,6-dithien-2-yl-2,5-bis(6-(1,1,1,3,5,5,5-heptamethyltrisiloxan-3-yl)hexyl)-pyrrolo[3,4-c]pyrrole-1,4-dione-5',5''-diyl-alt-3-(5-(selenophene-2-yl)) (PTDPPSe-Si). Isolated yield of polymer PTDPPSe-Si = 150 mg (75%). GPC analysis $M_n = 269.4$ kg/mol, $M_w = 1,180.8$ kg/mol, and PDI = 4.38 (against PS standard). $M_n = 122.3$ kg/mol, $M_w = 441.1$ kg/mol, and PDI = 3.58 (against PS standard) obtained by room temperature GPC and $M_n = 20.3$ kg/mol, $M_w = 100.0$ kg/mol, and PDI = 4.93 (against PS standard) measured by high-temperature GPC at 150 °C with 1,2,4-trichlorobenzene as eluent. $^1\text{H NMR}$ ($\text{C}_2\text{D}_2\text{Cl}_4$, 600 MHz, 348 K): δ ppm 9.07–8.54 (br, 2H), 7.49–6.67 (br, 4H), 4.17–3.74 (br, 4H), 1.67–1.01 (br, 16H), 0.44 (–0.24) (br, 46H). Anal. Calcd for $\text{C}_{44}\text{H}_{74}\text{N}_2\text{O}_6\text{S}_2\text{SeSi}_6$: C, 50.88; H, 7.18; N, 2.70; S, 6.17. Found: C, 50.64; H, 6.94; N, 2.75.

ASSOCIATED CONTENT

Supporting Information

Complete synthetic procedures and characterization of all the intermediates, additional figures (cyclic voltammetry plots, additional AFM and TEM images, and charge transport characteristics), TFT fabrication and testing, and AFM and TEM characterizations. This material is available free of charge via the Internet at <http://pubs.acs.org>.

AUTHOR INFORMATION

Corresponding Author

joonhoh@unist.ac.kr; yang@unist.ac.kr

Author Contributions

[§]These authors contributed equally.

Notes

The authors declare no competing financial interest.

ACKNOWLEDGMENTS

This work was supported by the National Research Foundation of Korea (NRF) funded by the Korean Government (MEST) (Grant No.: 2010-0002494, 2010-0019408, 2010-0026916, 2011-0026424, 2011-0017174) and Global Frontier Research Center for Advanced Soft Electronics (Grant No.: 2011-0031628).

REFERENCES

- Yan, H.; Chen, Z. H.; Zheng, Y.; Newman, C.; Quinn, J. R.; Dotz, F.; Kastler, M.; Facchetti, A. *Nature* **2009**, *457*, 679.
- McCulloch, I.; Heeney, M.; Bailey, C.; Genevicius, K.; Macdonald, I.; Shkunov, M.; Sparrowe, D.; Tierney, S.; Wagner, R.; Zhang, W. M.; Chabiny, M. L.; Kline, R. J.; McGehee, M. D.; Toney, M. F. *Nat. Mater.* **2006**, *5*, 328.
- Dhoot, A. S.; Yuen, J. D.; Heeney, M.; McCulloch, I.; Moses, D.; Heeger, A. J. *Proc. Natl. Acad. Sci. U.S.A.* **2006**, *103*, 11834.
- Pan, H.; Li, Y.; Wu, Y.; Liu, P.; Ong, B. S.; Zhu, S.; Xu, G. *J. Am. Chem. Soc.* **2007**, *129*, 4112.
- Lee, J.; Cho, S.; Seo, J. H.; Anant, P.; Jacob, J.; Yang, C. *J. Mater. Chem.* **2012**, *22*, 1504.
- Lee, J.; Han, A.-R.; Hong, J.; Seo, J. H.; Oh, J. H.; Yang, C. *Adv. Funct. Mater.* **2012**, *22*, 4128.
- Lee, J.; Cho, S.; Yang, C. *J. Mater. Chem.* **2011**, *21*, 8528.
- Cho, S.; Lee, J.; Tong, M.; Seo, J. H.; Yang, C. *Adv. Funct. Mater.* **2011**, *21*, 1910.
- Rogers, J. A.; Bao, Z.; Baldwin, K.; Dodabalapur, A.; Crone, B.; Raju, V. R.; Kuck, V.; Katz, H.; Amundson, K.; Ewing, J.; Drzaic, P. *Proc. Natl. Acad. Sci. U.S.A.* **2001**, *98*, 4835.
- Subramanian, V.; Chang, P. C.; Lee, J. B.; Molesa, S. E.; Volkman, S. K. *IEEE Trans. Compon., Packag. Technol.* **2005**, *28*, 742.
- Someya, T.; Kato, Y.; Sekitani, T.; Iba, S.; Noguchi, Y.; Murase, Y.; Kawaguchi, H.; Sakurai, T. *Proc. Natl. Acad. Sci. U.S.A.* **2005**, *102*, 12321.

- (12) Boudreault, P.-L. T.; Najari, A.; Leclerc, M. *Chem. Mater.* **2010**, *23*, 456.
- (13) McCulloch, I.; Heeney, M.; Chabiny, M. L.; DeLongchamp, D.; Kline, R. J.; Cölle, M.; Duffy, W.; Fischer, D.; Gundlach, D.; Hamadani, B.; Hamilton, R.; Richter, L.; Salleo, A.; Shkunov, M.; Sparrowe, D.; Tierney, S.; Zhang, W. *Adv. Mater.* **2009**, *21*, 1091.
- (14) Lu, G.; Usta, H.; Risko, C.; Wang, L.; Facchetti, A.; Ratner, M. A.; Marks, T. J. *J. Am. Chem. Soc.* **2008**, *130*, 7670.
- (15) Chua, L.-L.; Zaumseil, J.; Chang, J.-F.; Ou, E. C. W.; Ho, P. K. H.; Sirringhaus, H.; Friend, R. H. *Nature* **2005**, *434*, 194.
- (16) Zaumseil, J.; Sirringhaus, H. *Chem. Rev.* **2007**, *107*, 1296.
- (17) Fan, J.; Yuen, J. D.; Wang, M.; Seifert, J.; Seo, J. H.; Mohebbi, A. R.; Zakhidov, D.; Heeger, A.; Wudl, F. *Adv. Mater.* **2012**, *24*, 2186.
- (18) Zhang, W.; Smith, J.; Watkins, S. E.; Gysel, R.; McGehee, M.; Salleo, A.; Kirkpatrick, J.; Ashraf, S.; Anthopoulos, T.; Heeney, M.; McCulloch, I. *J. Am. Chem. Soc.* **2010**, *132*, 11437.
- (19) Tsao, H. N.; Cho, D. M.; Park, I.; Hansen, M. R.; Mavrinskiy, A.; Yoon, D. Y.; Graf, R.; Pisula, W.; Spiess, H. W.; Müllen, K. *J. Am. Chem. Soc.* **2011**, *133*, 2605.
- (20) Li, Y.; Singh, S. P.; Sonar, P. *Adv. Mater.* **2010**, *22*, 4862.
- (21) Li, Y.; Sonar, P.; Singh, S. P.; Soh, M. S.; van Meurs, M.; Tan, J. J. *Am. Chem. Soc.* **2011**, *133*, 2198.
- (22) Ha, J. S.; Kim, K. H.; Choi, D. H. *J. Am. Chem. Soc.* **2011**, *133*, 10364.
- (23) Chen, H.; Guo, Y.; Yu, G.; Zhao, Y.; Zhang, J.; Gao, D.; Liu, H.; Liu, Y. *Adv. Mater.* **2012**, *24*, 4618.
- (24) Babel, A.; Zhu, Y.; Cheng, K. F.; Chen, W. C.; Jenekhe, S. A. *Adv. Funct. Mater.* **2007**, *17*, 2542.
- (25) Meijer, E. J.; de Leeuw, D. M.; Setayesh, S.; van Veenendaal, E.; Huisman, B. H.; Blom, P. W. M.; Hummelen, J. C.; Scherf, U.; Klapwijk, T. M. *Nat. Mater.* **2003**, *2*, 678.
- (26) Dodabalapur, A.; Katz, H. E.; Torsi, L.; Haddon, R. C. *Science* **1995**, *269*, 1560.
- (27) Chen, Z.; Lemke, H.; Albert-Seifried, S.; Caironi, M.; Nielsen, M. M.; Heeney, M.; Zhang, W.; McCulloch, I.; Sirringhaus, H. *Adv. Mater.* **2010**, *22*, 2371.
- (28) Swensen, J. S.; Soci, C.; Heeger, A. J. *Appl. Phys. Lett.* **2005**, *87*, 253511.
- (29) Li, H.; Mei, J.; Ayzner, A. L.; Toney, M. F.; Tok, J. B. H.; Bao, Z. *Org. Electron.* **2012**, *13*, 2450.
- (30) Sonar, P.; Singh, S. P.; Li, Y.; Soh, M. S.; Dodabalapur, A. *Adv. Mater.* **2010**, *22*, 5409.
- (31) Chen, Z.; Lee, M. J.; Shahid Ashraf, R.; Gu, Y.; Albert-Seifried, S.; Meedom Nielsen, M.; Schroeder, B.; Anthopoulos, T. D.; Heeney, M.; McCulloch, I.; Sirringhaus, H. *Adv. Mater.* **2012**, *24*, 647.
- (32) Yuen, J. D.; Fan, J.; Seifert, J.; Lim, B.; Hufschmid, R.; Heeger, A. J.; Wudl, F. *J. Am. Chem. Soc.* **2011**, *133*, 20799.
- (33) Usta, H.; Newman, C.; Chen, Z.; Facchetti, A. *Adv. Mater.* **2012**, *24*, 3678.
- (34) Roelofs, W. S. C.; Mathijssen, S. G. J.; Bijleveld, J. C.; Raiteri, D.; Geuns, T. C. T.; Kemerink, M.; Cantatore, E.; Janssen, R. A. J.; de Leeuw, D. M. *Appl. Phys. Lett.* **2011**, *98*, 203301.
- (35) Baeg, K.-J.; Kim, J.; Khim, D.; Caironi, M.; Kim, D.-Y.; You, I.-K.; Quinn, J. R.; Facchetti, A.; Noh, Y.-Y. *ACS Appl. Mater. Interfaces* **2011**, *3*, 3205.
- (36) Xin, H.; Guo, X.; Kim, F. S.; Ren, G.; Watson, M. D.; Jenekhe, S. A. *J. Mater. Chem.* **2009**, *19*, 5303.
- (37) Steckler, T. T.; Zhang, X.; Hwang, J.; Honeyager, R.; Ohira, S.; Zhang, X.-H.; Grant, A.; Ellinger, S.; Odom, S. A.; Sweat, D.; Tanner, D. B.; Rinzler, A. G.; Barlow, S.; Brédas, J.-L.; Kippelen, B.; Marder, S. R.; Reynolds, J. R. *J. Am. Chem. Soc.* **2009**, *131*, 2824.
- (38) Osaka, I.; Abe, T.; Shinamura, S.; Miyazaki, E.; Takimiya, K. *J. Am. Chem. Soc.* **2010**, *132*, 5000.
- (39) Hou, J.; Chen, H.-Y.; Zhang, S.; Li, G.; Yang, Y. *J. Am. Chem. Soc.* **2008**, *130*, 16144.
- (40) Chen, C.-P.; Chan, S.-H.; Chao, T.-C.; Ting, C.; Ko, B.-T. *J. Am. Chem. Soc.* **2008**, *130*, 12828.
- (41) Thompson, B. C.; Fréchet, J. M. J. *Angew. Chem., Int. Ed.* **2008**, *47*, 58.
- (42) Wienk, M. M.; Turbiez, M.; Gilot, J.; Janssen, R. A. J. *Adv. Mater.* **2008**, *20*, 2556.
- (43) Dennler, G.; Scharber, M. C.; Brabec, C. J. *Adv. Mater.* **2009**, *21*, 1323.
- (44) Osaka, I.; Sauvé, G.; Zhang, R.; Kowalewski, T.; McCullough, R. D. *Adv. Mater.* **2007**, *19*, 4160.
- (45) Wang, M.; Hu, X.; Liu, P.; Li, W.; Gong, X.; Huang, F.; Cao, Y. *J. Am. Chem. Soc.* **2011**, *133*, 9638.
- (46) Son, H. J.; Wang, W.; Xu, T.; Liang, Y.; Wu, Y.; Li, G.; Yu, L. *J. Am. Chem. Soc.* **2011**, *133*, 1885.
- (47) Lei, T.; Cao, Y.; Fan, Y.; Liu, C.-J.; Yuan, S.-C.; Pei, J. *J. Am. Chem. Soc.* **2011**, *133*, 6099.
- (48) Gidron, O.; Dadvand, A.; Sheynin, Y.; Bendikov, M.; Perepichka, D. F. *Chem. Commun.* **2011**, *47*, 1976.
- (49) Grimsdale, A. C.; Leok Chan, K.; Martin, R. E.; Jokisz, P. G.; Holmes, A. B. *Chem. Rev.* **2009**, *109*, 897.
- (50) Carsten, B.; He, F.; Son, H. J.; Xu, T.; Yu, L. *Chem. Rev.* **2011**, *111*, 1493.
- (51) Zhou, H.; Yang, L.; Stuart, A. C.; Price, S. C.; Liu, S.; You, W. *Angew. Chem., Int. Ed.* **2011**, *50*, 2995.
- (52) Varotto, A.; Treat, N. D.; Jo, J.; Shuttle, C. G.; Batara, N. A.; Brunetti, F. G.; Seo, J. H.; Chabiny, M. L.; Hawker, C. J.; Heeger, A. J.; Wudl, F. *Angew. Chem., Int. Ed.* **2011**, *50*, 5166.
- (53) Wang, E.; Ma, Z.; Zhang, Z.; Vandewal, K.; Henriksson, P.; Inganäs, O.; Zhang, F.; Andersson, M. R. *J. Am. Chem. Soc.* **2011**, *133*, 14244.
- (54) Mei, J. G.; Kim, D. H.; Ayzner, A. L.; Toney, M. F.; Bao, Z. *J. Am. Chem. Soc.* **2011**, *133*, 20130.
- (55) Shahid, M.; McCarthy-Ward, T.; Labram, J.; Rossbauer, S.; Domingo, E. B.; Watkins, S. E.; Stingelin, N.; Anthopoulos, T. D.; Heeney, M. *Chem. Sci.* **2012**, *3*, 181.
- (56) Patra, A.; Bendikov, M. *J. Mater. Chem.* **2010**, *20*, 422.
- (57) Wijsboom, Y. H.; Patra, A.; Zade, S. S.; Sheynin, Y.; Li, M.; Shimon, L. J. W.; Bendikov, M. *Angew. Chem., Int. Ed.* **2009**, *48*, 5443.
- (58) Oh, J. H.; Sun, Y.-S.; Schmidt, R.; Toney, M. F.; Nordlund, D.; Könnemann, M.; Würthner, F.; Bao, Z. *Chem. Mater.* **2009**, *21*, 5508.
- (59) Schmidt, R.; Oh, J. H.; Sun, Y.-S.; Deppisch, M.; Krause, A.-M.; Radacki, K.; Braunschweig, H.; Könnemann, M.; Erk, P.; Bao, Z.; Würthner, F. *J. Am. Chem. Soc.* **2009**, *131*, 6215.
- (60) Lee, O. P.; Yiu, A. T.; Beaujuge, P. M.; Woo, C. H.; Holcombe, T. W.; Millstone, J. E.; Douglas, J. D.; Chen, M. S.; Fréchet, J. M. J. *Adv. Mater.* **2011**, *23*, 5359.
- (61) Dantlgraber, G.; Eremin, A.; Diele, S.; Hauser, A.; Kresse, H.; Pelzl, G.; Tschierske, C. *Angew. Chem., Int. Ed.* **2002**, *41*, 2408.
- (62) Seitz, D. E.; Lee, S. H.; Hanson, R. N.; Bottaro, J. C. *Synth. Commun.* **1983**, *13*, 121.
- (63) Ashraf, R. S.; Kronemeijer, A. J.; James, D. I.; Sirringhaus, H.; McCulloch, I. *Chem. Commun.* **2012**, *48*, 3939.
- (64) Sun, B.; Hong, W.; Aziz, H.; Li, Y. *J. Mater. Chem.* **2012**, *22*, 18950.
- (65) Gao, Y. *Acc. Chem. Res.* **1999**, *32*, 247.
- (66) Ong, B. S.; Wu, Y.; Liu, P.; Gardner, S. J. *J. Am. Chem. Soc.* **2004**, *126*, 3378.
- (67) Rivnay, J.; Steyrlleuthner, R.; Jimison, L. H.; Casadei, A.; Chen, Z.; Toney, M. F.; Facchetti, A.; Neher, D.; Salleo, A. *Macromolecules* **2011**, *44*, 5246.
- (68) Becerril, H. A.; Roberts, M. E.; Liu, Z.; Locklin, J.; Bao, Z. *Adv. Mater.* **2008**, *20*, 2588.
- (69) Oh, J. H.; Lee, W.-Y.; Noe, T.; Chen, W.-C.; Könnemann, M.; Bao, Z. *J. Am. Chem. Soc.* **2011**, *133*, 4204.
- (70) Giri, G.; Verploegen, E.; Mannsfeld, S. C. B.; Atahan-Evrenk, S.; Kim, D. H.; Lee, S. Y.; Becerril, H. A.; Aspuru-Guzik, A.; Toney, M. F.; Bao, Z. *Nature* **2011**, *480*, 504.
- (71) Brédas, J.-L.; Beljonne, D.; Coropceanu, V.; Cornil, J. *Chem. Rev.* **2004**, *104*, 4971.
- (72) Sirringhaus, H. *Adv. Mater.* **2009**, *21*, 3859.
- (73) Kim, F. S.; Guo, X.; Watson, M. D.; Jenekhe, S. A. *Adv. Mater.* **2010**, *22*, 478.